Electronic Supplementary Material (ESI) for Environmental Science: Nano.

Fluorescent Plastic Nanoparticles to Track their Interaction and Fate in Physiological Environments

Jessica Caldwell[a], Roman Lehner[a], Sandor Balog[a], Christian Rhême[b], Xin Gao[b], Dedy Septiadi[a], Christoph Weder[a*], Alke Petri-Fink[a], Barbara Rothen-Rutishauser[a*]

[a]*Adolphe Merkle Institute, Université de Fribourg, Chemin des Verdiers 4, 1700 Fribourg, Switzerland*

[b]*Frewitt fabrique de machines SA, Route du Coteau 7, 1763 Granges-Paccot, Switzerland*

**Corresponding authors: Barbara Rothen-Rutishauser barbara.rothen@unifr.ch and Christoph Weder christoph.weder@unifr.ch*

Pages: 24

Figures: 11

Tables: 5

Table of Contents

Section S1: Material Production

Section S1.1: Materials

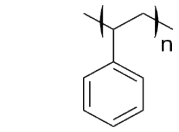

Polystyrene (PS)

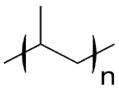

Polypropylene (PP)

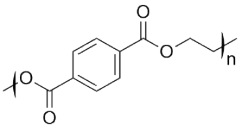

Polyethylene terephthalate (PET)

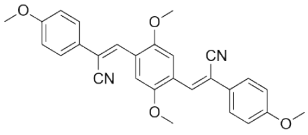

1,4-bis(α-cyano-4-methoxystyryl)-2,5-dimethoxybenzene (C1RG)

Figure S1: The NanoWitt-Lab mill (FREWITT SA, Switzerland) and chemical structure of the polymers and the thermostable fluorophore used in this study.

Section S1.2: Melt-Mixing Methods

Table S1: Material properties such as molecular weight (M_w) and density, dye mass (per 2.5 g of virgin polymer), and melt processing temperatures for each polymer. Values for the various material properties were obtained from the respective company that produced the virgin polymer pellets. The acronym n.r. indicates a value was not reported by the manufacturer.

Polymer	M_w (kDA)	Density (g/cm^3)	C1RG Mass per film (mg)	Processing Temperature (˚C)
Polypropylene (PP)	192,000	0.90	0.25	170
Polystyrene (PS)	190,000	n.r.	0.25	200
Poly(ethylene terephthalate) (PET)	n.r.	1.35	2.5	255

Section S2: Characterization of Pellets and Microparticles

Section S2.1: DSC Method

Virgin pellets, melt processed pellet controls, cryo-milled unlabeled microparticles, and cryo-milled fluorescent microparticles were placed into a DSC 2 Star System (Mettler Toledo, USA). Each sample of particles was subjected to two heating and two cooling cycles using heating and cooling rates of 10 °C per minute, with settings adjusted to account for differences in the anticipated transition temperatures of each material (Table S2). The same temperatures were utilized for labeled and unlabeled microparticle samples.

Table S2: Temperatures utilized for differential scanning calorimetry measurements of plastic pellets and microparticles.

Polymer	**Minimum Temperature (˚C)**	**Maximum Temperature (˚C)**
Polypropylene (PP)	-40	200
Polystyrene (PS)	25	250
Poly(ethylene terephthalate) (PET)	25	275

Section S2.2: DSC Results

The melt processing incorporation of the C1RG fluorophore and subsequent cryo-milling into plastic microparticles was possible for all materials utilized in the study. Upon completion of the melt

processing and cryo-milling for all materials, the impact of the melt processing treatment on the plastic microparticles' transition temperatures were assessed utilizing DSC (Figure S2).

The DSC traces of the virgin PS pellet, PS melt processed control, unlabeled PS microparticles, and the PSC1RG microparticles are virtually identical. As expected for this amorphous polymer, the only transition visible is the glass transition, which appears with a glass transition temperature (T_g) in agreement with values reported in literature to range from 100 ˚C to 107 ˚C [1] (*e.g.* near 102 ˚C for PSC1RG and unlabeled PS microparticles, near 108 ˚C for the melt processed PS control, and near 109 ˚C for the virgin PS).

The DSC traces of the virgin PP pellet, PP melt processed control, unlabeled PP microparticles, and PPC1RG microparticles are also practically identical. Crystallization temperatures (T_c) range from 115 ˚C for the virgin PP pellet to 116 ˚C (fist cooling) for the microparticles to 121 ˚C for the melt processed PP control. Melting temperatures (T_m) range from 159 ˚C (second heating) for the PPC1RG microparticles to 162 ˚C for the unlabeled PP microparticles to 164 ˚C for both pellet controls. These values are in good agreement with the value of 117 ˚C for the T_c and 160 ˚C for the T_m reported in literature [2]. No glass transition could be discerned for PP (according to literature around -10 ˚C [2]), presumably on account of the high crystallinity.

Interestingly, the DSC traces of the PET samples show noticeable differences. The first cooling/second heating traces of the unlabeled microparticles show a broad T_c around 185 ˚C upon cooling, a T_g around 80 °C, and a T_m of 244 ˚C upon heating. The PETC1RG microparticles show a different crystallization behavior. The first cooling trace reveals that the crystallization peak is much sharper and T_c is higher (205 °C) than in the unlabeled material, while the integration of the melting endotherm in the second heating reveals a slightly higher crystallinity than in the unlabeled material. A similar trend could be seen for the melt processed PET control; with a sharp crystallization peak at 205 °C and a T_m of 251 °C. A

comparison of the DSC results for the microparticle and melt processed control samples with the DSC data for the virgin pellet revealed that there was a striking difference in the crystallization temperatures and peak shapes for the samples; with the virgin sample having a very broad T_c peak at 150 °C and a T_m of 248 °C. Thus, the peak sharpening and increase in the T_c values for the milled and melt processed samples is likely the result of a reduction of the molecular weight of the polymer; a trend which was also reported by Romão *et al.* for recycled PET samples [3]. Depending on the type of material processing the sample underwent prior to DSC measurements, two key sources of this damage should be considered. The first is a reduction in the molecular weight as a result of the mechanical forces the material is exposed to during the milling procedure; resulting in the increased T_c observed for the unlabeled PET microplastic sample. The second likely cause of the increase in the T_c of the melt processed samples (*i.e.* the melt processed PET control pellet and the PETC1RG microparticles) is chain scission as the result of the thermo-mechanical forces that the material is subjected to during the melt mixing procedure; a phenomenon also reported by Spinacé *et al.* [4]. However, in the study conducted by Spinacé *et al.* a maximum T_c shift of 40 °C was observed; a difference which is likely the result of the pre-drying step conducted at 160 °C prior to their material processing [4]. This additional step can be introduced into future protocols looking to work with PET samples to ensure that the damage to the polymer chains as a result of moisture present during the melt processing procedure [5] is mitigated.

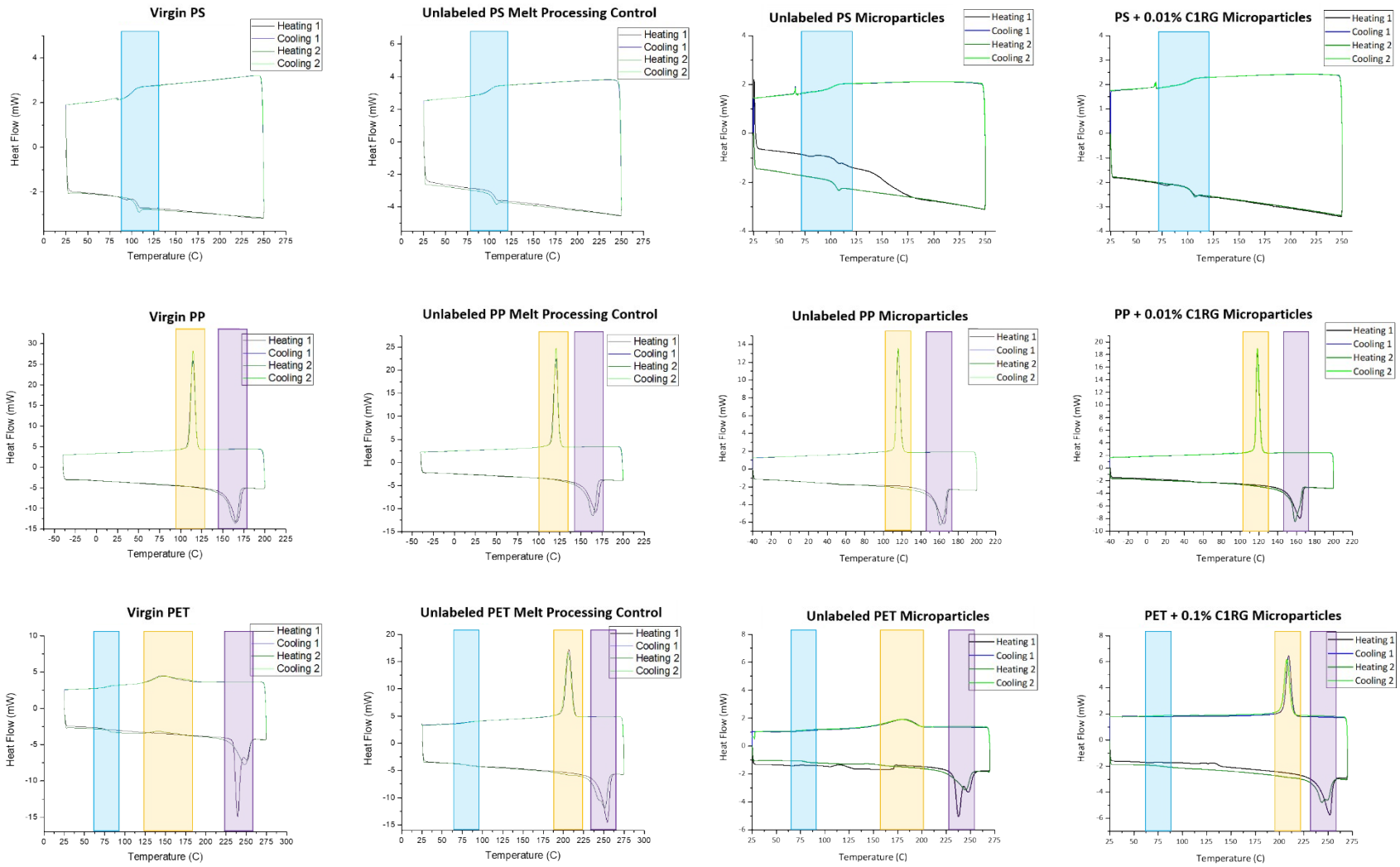

Figure S2: Differential Scanning Calorimetry plots recorded for virgin plastic pellets, melt processed plastic pellet controls, unlabeled plastic microparticles, and

fluorescent plastic microparticles. Temperatures in which glass transitions occur are highlighted in blue, regimes in which crystallizations occur are highlighted in orange, and ranges in which samples melt are highlighted in purple. Exothermic events are shown up and all traces were recorded at heating and cooling rate of 10 °C per minute. Data quoted in the text were extracted from the first cooling and second heating trace and the first heating was merely used to erase any sample history.

Table S3: A summary of the transition temperature ranges measured with DSC for each polymer type.

Material	T_g (˚C)	T_m (˚C)	T_c (˚C)
Virgin PET Pellet	80	248	150
Melt Processed PET Control	85	251	205
Unlabeled PET Microparticles	80	244	185
PETC1RG Microparticles	75	248	205
Virgin PP Pellet	_	164	115
Melt Processed PP Control	_	164	121
Unlabeled PP Microparticles	_	162	116
PPC1RG Microparticles	_	159	116
Virgin PS Pellet	109	_	_
Melt Processed PS Control	108	_	_
Unlabeled PS Microparticles	102	_	_
PSC1RG Microparticles	102	_	_

Section S2.3: Microparticle Imaging

The impact of the materials' thermomechanical properties on the mechanical disintegration during milling and the morphology of the particles produced can clearly be seen in the SEM images (Figure S3).

Additional images of the particles, obtained with cLSM, served two purposes. First, they allow for further analysis of the particle shape. Second, fluorescent and bright field scanning modes could be used to assess whether fluorophore incorporation was homogenous in the plastic microparticles, and whether the unlabeled plastics display any fluorescence of their own (*i.e.* as a result of the presence of additives such as optical brighteners). Particles composed of all unlabeled plastic types showed no fluorescence when imaged with an excitation laser wavelength of 488 nm. Particles which were melt-mixed with C1RG showed fluorescence at this wavelength. Additionally, the particles displayed this fluorescence in a homogenous manner, with a good correlation between the shape of the plastic microparticles in bright field images and the shape observed in the fluorescent images. Fluorescence was observed only for particles that were within the focal plane during imaging.

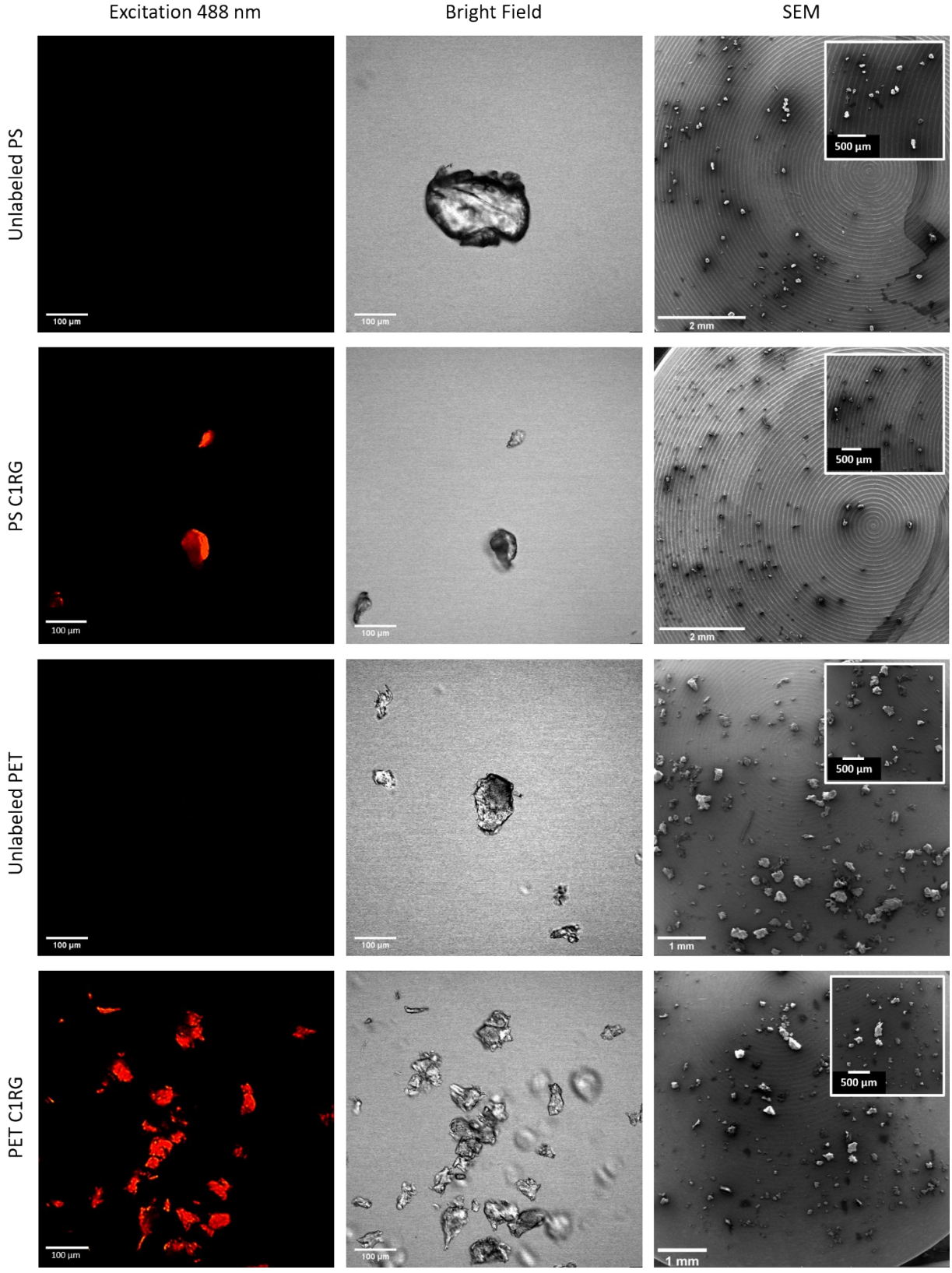
Excitation 488 nm
Bright Field
SEM
Unlabeled PS
PS C1RG
Unlabeled PET
PET C1RG
100 µm
2 mm
500 µm
1 mm

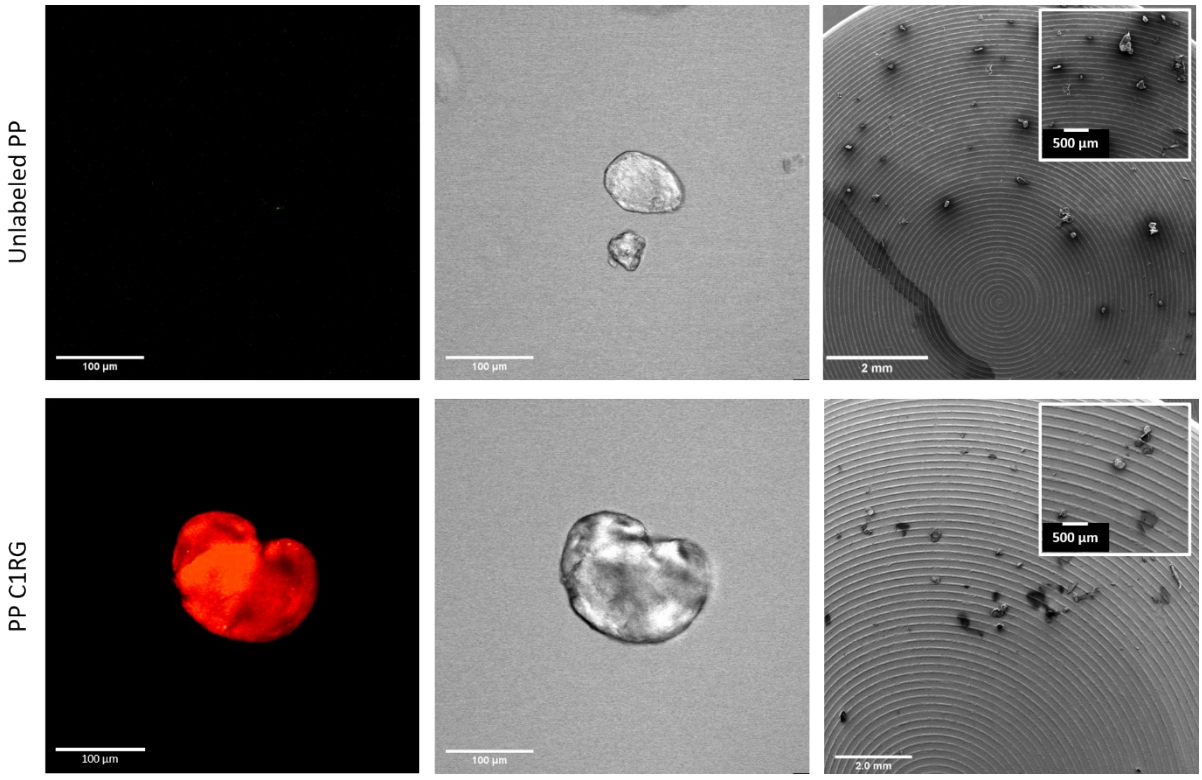

Figure S3: Representative images of polypropylene, poly(ethylene terephthalate), and polystyrene microparticles obtained utilizing confocal laser scanning microscopy with a fluorescent excitation of 488 nm, shown in red (left column), confocal laser scanning microscopy in bright field mode (central column), and scanning electron microscopy (right column). Inset: representative particles at higher magnification showing the particles' surface.

Section S2.4: Contact Angle Method

Thin films of the C1RG labelled and unlabeled plastic microparticles were prepared by compression molding 0.5 g of each sample between Kapton sheets in a hot press (Carver, USA) at 200 (PS), 170 (PP), or 255 (PET) °C with a pressure of 2 metric tons for 1 minute and then 5 metric tons for an additional minute. The films were removed from the press and cooled to ambient temperature between the Kapton sheets. The thin films were then placed in a Dataphysics OCA 15Pro contact angle instrument (Filderstadt, Germany) equipped with an IDS UI-222xSE-M R3 camera (Obersulm, Germany) and the accompanying SCA20 software (version 4.5.15; Filderstadt, Germany) was utilized to measure the

contact angle of 2 µl droplets of MilliQ water. For each thin film, 5 measurements were obtained and averaged to yield a final contact angle measurement and standard deviation.

Section S2.5: Contact Angle Results

Table S4: Final average contact angle measured for thin films of each plastic microparticle type compared to literature values.

Polymer	Average Contact Angle	Standard Deviation	Reported Literature Values
Unlabeled PP	94°	4°	90° [6]
PPC1RG	91°	4°	_
Unlabeled PS	83°	6°	86° [7]
PSC1RG	86°	8°	_
Unlabeled PET	83°	5°	79° [6]
PETC1RG	81°	3°	_

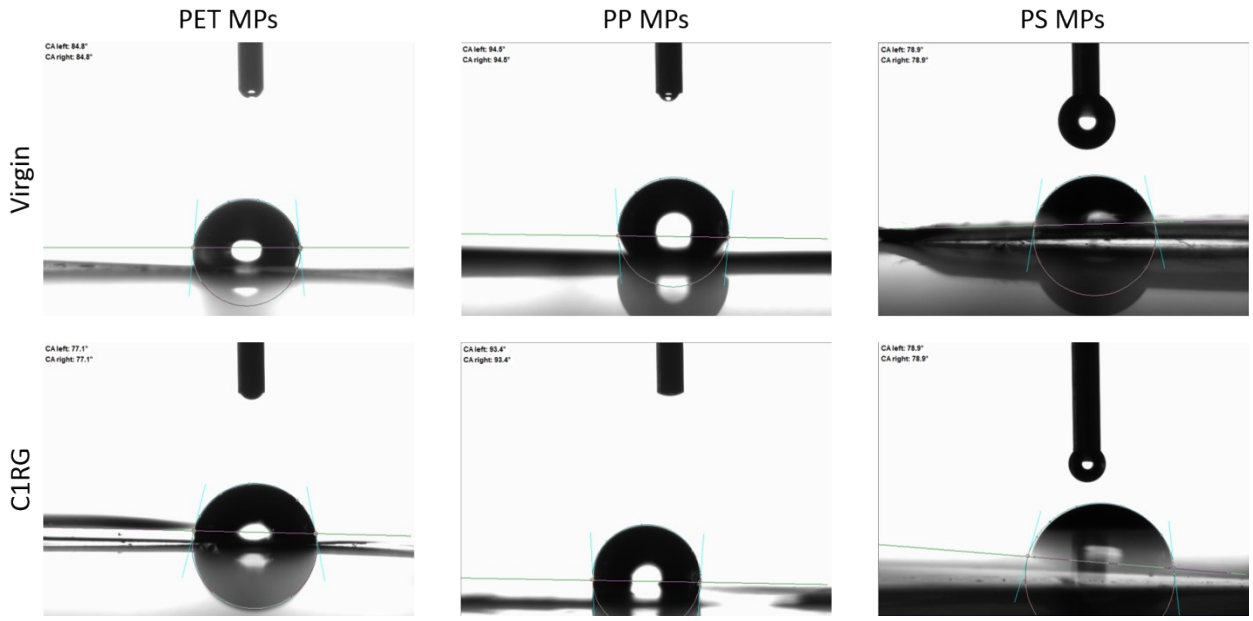

Figure S4: Representative images of 2 µl water droplets utilized to obtain contact angle measurements for thin films of each plastic particle type.

Section S3: Attenuated Total Reflection Fourier Transform Infrared Spectroscopy of All Materials

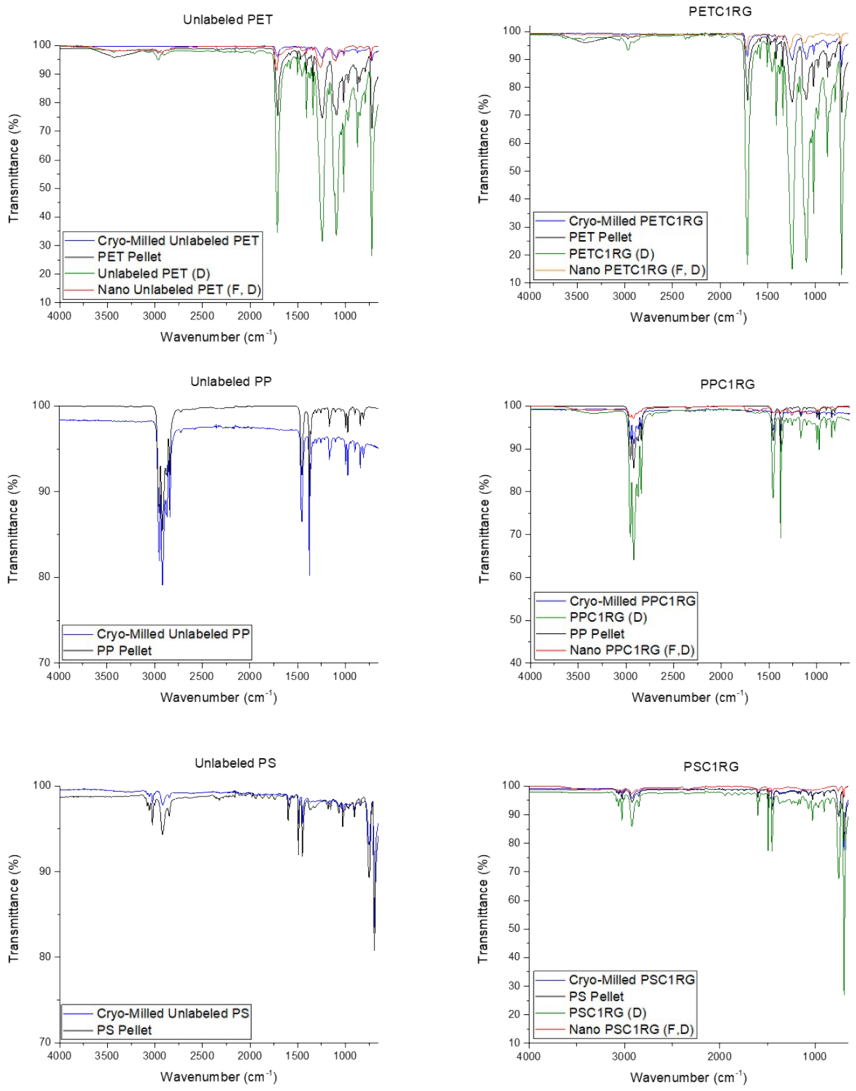

Figure S5: Chemical fingerprints obtained for all materials used in the study. Fingerprints were obtained after each major material processing step (e.g. milling, filtering) to ensure plastic particles were present in the studied dispersions. A (D) in the figure legend indicates the sample was dialyzed prior to obtaining its chemical fingerprint, while (F, D) indicates both filtration and dialysis. PSC1RG has a small peak at 3000 cm^{-1} as a result of the aromatic C-H stretch present in the ring structure, with an additional peak present near 2950 cm^{-1} as a result of the C-H stretch from the remaining single bonds in the backbone, and peaks from 1450 cm^{-1} to 1600 cm^{-1} as a result of the C=C stretch in the aromatic ring [8]. PPC1RG had a single, broad peak at 2950 cm^{-1} as a result of C-H stretching in the

alkane backbone and multiple sharper peaks between 1470 cm^{-1} and 1450 cm^{-1}as a result of C-H bending from the alkanes. Smaller peaks near 715-725 cm^{-1} are seen as the result of -CH_2 groups [8]. The PET and PETC1RG spectra show sharp peaks near 1640-1670 cm^{-1} as a result of the alkene C=C stretch, a peak near 1020-1070 cm^{-1} and 1200-1275 cm^{-1} as a result of the C-O-C stretch of the ethers present with the aromatic rings, and multiple peaks present below 1,000 cm^{-1} as a result of the multiple para-aromatic rings present within the backbone [8].

Section S4: Characterization of Plastic Nanoparticles

Section S4.1: Plastic Nanoparticle Imaging

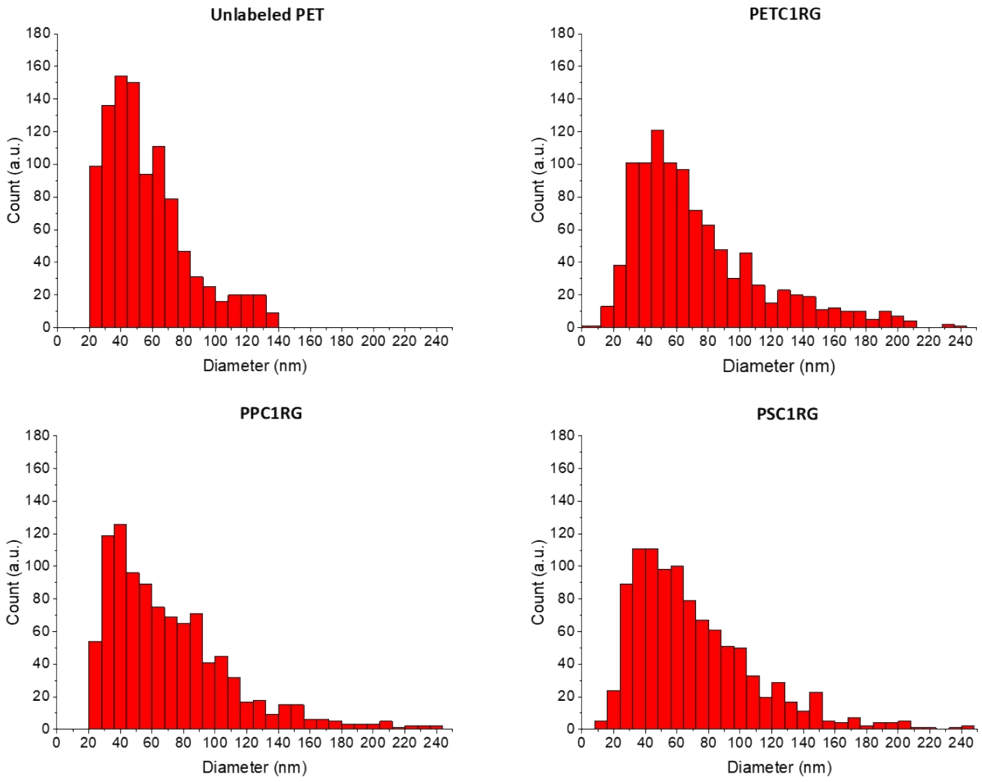

Figure S6: Histograms of the sizes measured for the plastic nanoparticles during scanning electron microscopy analysis. Each histogram represents measurements obtained from 1000 particles.

Section S4.2: Zeta Potential Methods

All zeta potential (ζ-potential) measurements were obtained at room temperature with a 90Plus particle size analyzer (Brookhaven, USA). Particles were suspended in MilliQ water at neutral pH.

Section S4.3: Zeta Potential Results

The aggregates which could be seen in microscopy images highlighted the need to assess the colloidal stability and size of the particles in their suspended state. Thus, ζ-potentials for the nanoparticle dispersions were measured (Table S5). Unlabeled and C1RG labelled PET nanoparticles, with ζ-potential values near the +/- 30 mV commonly reported as the indicator for good particle stability [9] when suspended in MilliQ water, required no additional treatment prior to DLS and DDLS measurements. PSC1RG and PPC1RG nanoparticles rapidly sedimented upon dialysis completion. Thus, accurate ζ-potential and light scattering measurements could not be obtained for these particles until they were re-stabilized with 1% SDS. ζ-potential values of -43 mV for PSC1RG and -36 mV for PPC1RG were obtained after surfactant stabilization (Table S5).

Table S5: A summary of the ζ-potential values for all stable particle suspensions

Polymer	ζ-Potential (mV)
PPC1RG	-36*
PSC1RG	-43*
Unlabeled PET	-29
PETC1RG	-26

** Indicates particle stabilization with 1% SDS was required to obtain accurate measurements.*

Section S4.4: Polarized and Depolarized Dynamic Light Scattering (DLS, DDLS) Methods

Light scattering data were collected for the filtered, dialyzed plastic nanoparticle dispersions, both with and without stabilization with 1% SDS, at constant temperature (21 °C) on a commercial goniometer instrument (3D LS Spectrometer, LS Instruments AG, Switzerland). Scattering angles ranged from Θ = 30°

to Θ = 150° with 10 measurements of 30 seconds taken per angle. The incident beam was formed by a linearly polarized and collimated laser beam (Cobolt 05-01 diode pumped solid state laser, λ = 660 nm, *P max.* = 500 mW), and the scattered light was collected by single-mode optical fibers equipped with integrated collimation optics. The incoming laser beam passed through a Glan-Thompson polarizer with an extinction ratio of 10^{-6}, and another Glan-Thompson polarizer with an extinction ratio of 10^{-8} was placed in front of the collection optics (for polarized and depolarized light scattering) [10]. To construct the intensity auto-correlation function $g_2(t)$, the collected light was coupled into two APD detectors via laser-line filters (Perkin Elmer, Single Photon Counting Module), and their outputs were fed into a multi-tau digital correlator (LSI Correlator LS Instruments AG, Switzerland). To improve the signal-to-noise ratio and to eliminate the impact of detector after-pulsing on $g_2(t)$ at early lag times (<1 μs), necessary for the cumulant analysis, these two detectors were cross-correlated. The field auto-correlation function was obtained via the Siegert relation (eqn. 1):

$$g_1(t) = \sqrt{g_2(t) - 1}\,.$$

Without any modification made, the photon count traces of one of the detectors were obtained through the same detection line as above, at a sampling rate of nearly 19 Hz. To maximize the available accuracy and precision, the data analysis—akin to the well-known cumulant analysis resulting in the estimation of the scattering intensity-weighted average hydrodynamic radius, also known as z-average, included an unbiased classification of data quality based on the statistical analysis of photon counts [11-14].

The plastic nanoparticles were also dispersed in cell culture medium (cDMEM supplemented with proteins; 1.2 μg mL^{-1} PSC1RG; 2.1 μg mL^{-1} PPC1RG; 10.2 μg mL^{-1} PETC1RG; 7.9 μg mL^{-1} unlabeled PET), and if the scattering intensity from the media itself was not less than 5% compared to that of the particles, polarized DLS spectra (10 measurements of 30 seconds at Θ = 90˚) were analyzed as reported elsewhere [15].

Section S4.5: Light Scattering in MilliQ Water

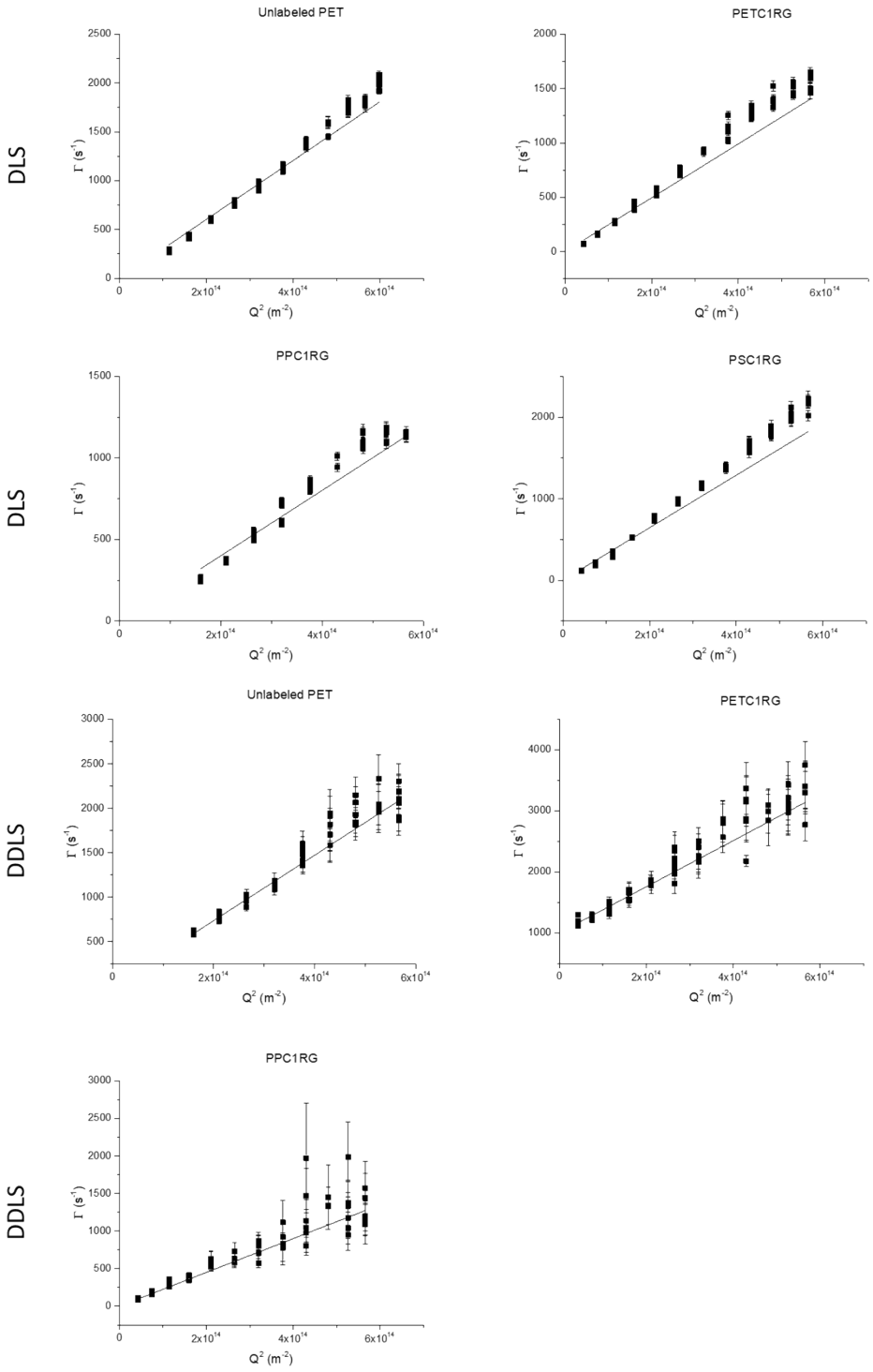

Figure S7: Plots of the decay constant (Γ) of the particles against their squared momentum transfer (Q^2) which were used to calculate the average hydrodynamic radius (R_H) of every suspension. As the PSC1RG milled in this

experiment was amorphous, the nanoparticles of this material did not scatter light in an anisotropic manner and could not be seen in DDLS.

Section S4.6: Light Scattering in Cell Culture Media

Prior to exposing the particles to cell cultures, deeper understanding of the behavior of plastic nanoparticles in cell culture media containing serum was required. It was determined that DDLS measurements were not suitable for characterization of the highly amorphous PSC1RG nanoparticles (Figure S7) as they have no crystalline regions; a feature that is a necessary requirement to obtain the anisotropic scattering needed to size with DDLS. Thus, DLS measurements were utilized to measure the hydrodynamic radii of the plastic nanoparticles dispersed in cell culture media. As the concentration and size of the proteins within the cell culture medium is relatively constant, the scattering of the proteins and other components present within the cell culture medium are assumed to remain static even after the addition of the nanoparticles. This assumption relies on the considerably higher concentration of proteins present in cell culture medium (3.0-4.5 g L^{-1} [16]) compared to the concentration of the nanoparticles added (0.01021 g L^{-1} for PETC1RG particles, 0.0012 g L^{-1} for PSC1RG particles, and 0.00214 g L^{-1} for PPC1RG particles). At such high concentration differences, the amount of proteins interacting with the surface of the plastic nanoparticles, resulting in the formation of a protein corona, is negligible. Therefore, this interaction is assumed to have no effect and the overall behavior and composition of the cell culture media and the scattering of the proteins can be treated as static noise that is accounted for by subtracting the corresponding autocorrelation function [17].

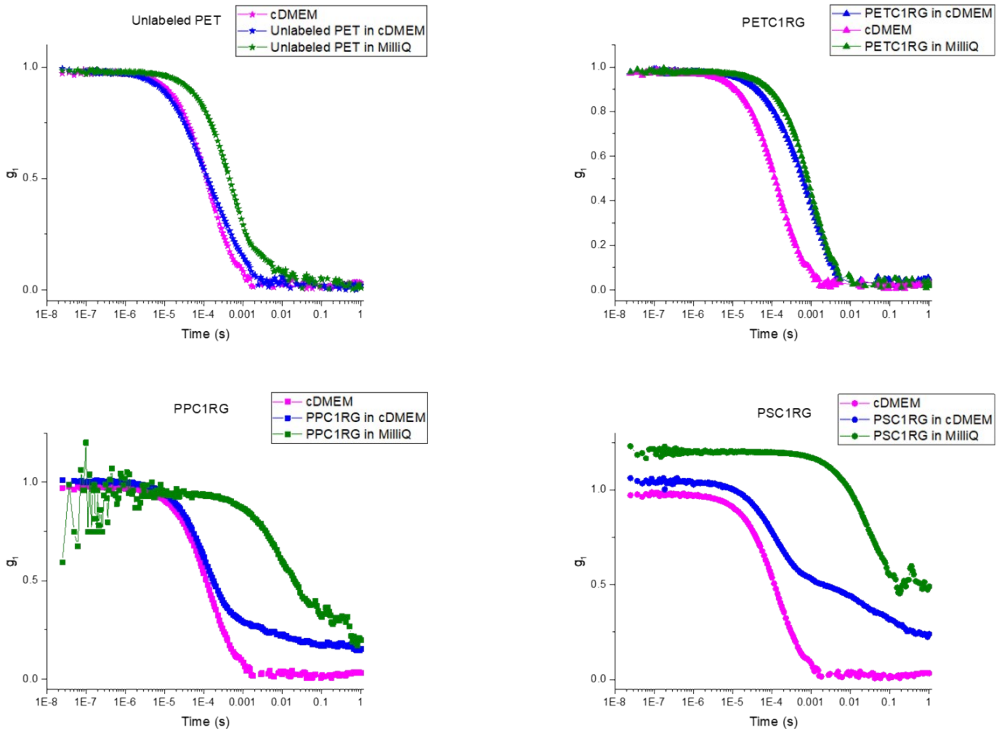

Figure S8: Field auto-correlation functions obtained for all particles dispersed in cDMEM. For each measurement, hydrodynamic radii for the proteins present in the media and for the particles dispersed in MilliQ water were obtained prior to their dispersion in the media. For comparison, the auto-correlation functions are presented for all 3 experimental conditions (cDMEM alone (pink), particles in MilliQ water (green), and particles in cDMEM (blue)).

Section S4.7: Nanoparticle Concentrations

The concentration of each sample was calculated using a modified version of the Sauerbrey equation (eqn. 2):

$$\Delta m = C_f * \Delta f$$

The change in crystal frequency, Δf, is given by eqn. 3:

$$\Delta f = f_0 - f_e$$

C_f is a constant value of 1.25 ng Hz^{-1} that accounts for the crystal area and various physical properties of the quartz [18]. Δm is the change in the mass after deposition of the particles. f_0 is the crystal frequency prior to deposition, with f_e being the final stable frequency value (Figure S9).

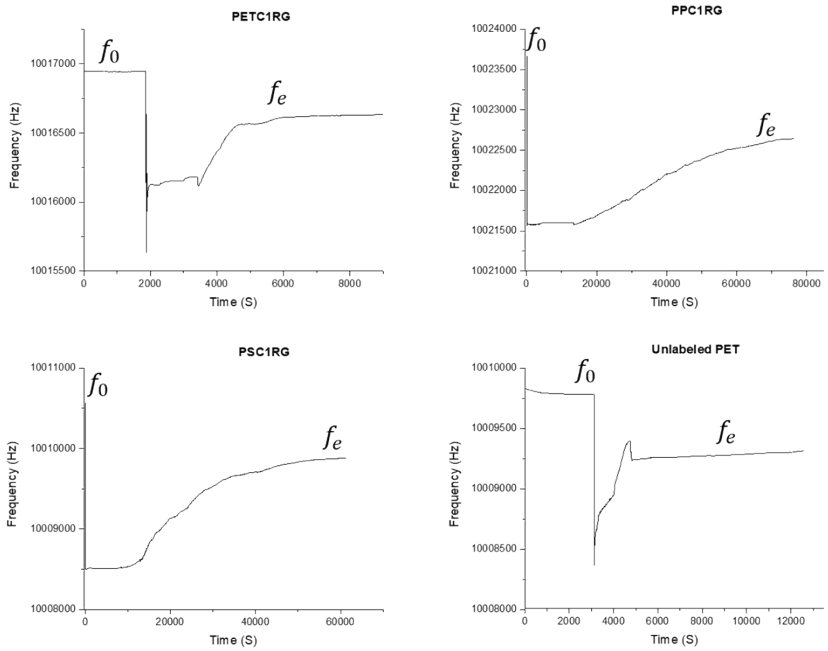

Figure S9: A representative quartz crystal microbalance plot obtained for a single concentration measurement of each nanoparticle dispersion. The initial baseline frequency and end frequency for the measurements have been labelled f_0 and f_e, respectively. A rapid drop in the frequency values is present as a result of the addition of the sample to the crystal at the beginning of the measurement.

S4.8: Lactate Dehydrogenase (LDH) Assay Results and C1RG Control Experiments

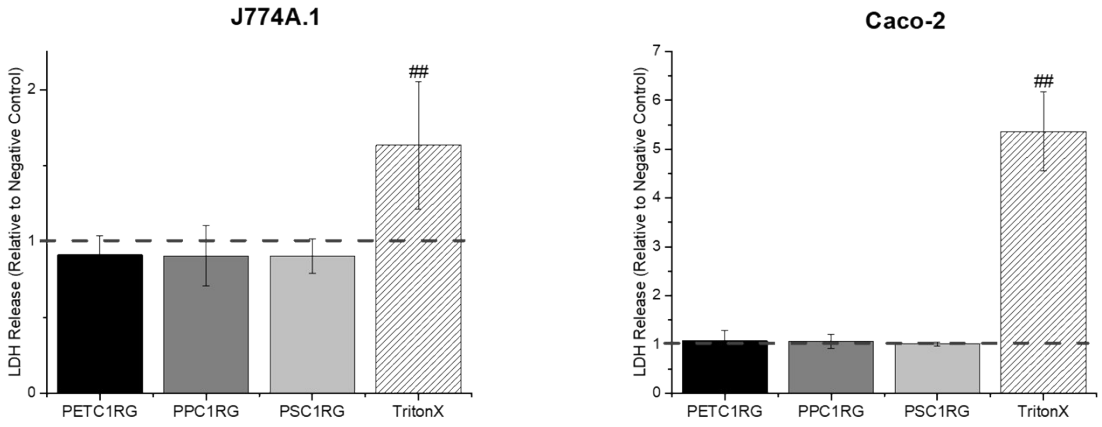

Figure S10: Lactate dehydrogenase assay data for the Caco-2 cells (right) and J774A.1 macrophages (left) utilized in the initial particle exposure studies. LDH measurements for cells exposed to plastic nanoparticles were averaged and normalized to the negative controls to obtain the final reported values. ## indicates a statistical difference from the negative control (n = 3, one-way ANOVA, Tukey, p = 0.05).

S4.9: C1RG Control Experiments with J774A.1 Cells

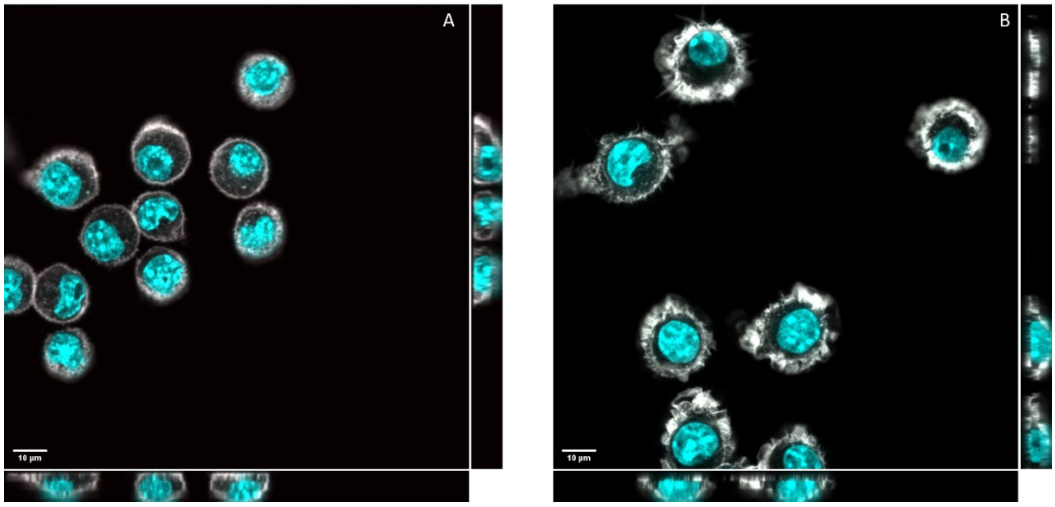

Figure S11: J774A.1 cells exposed to the highly hydrophobic free C1RG dye for 24 hours (A) and a negative control for comparison (B). DAPI is shown in cyan, rhodamine/phalloidin in white, and the channel used to excite C1RG in red. Scale bar: 10 µm.

Section S5: Additional References

1. Rieger, J., *The glass transition temperature of polystyrene.* Journal of thermal analysis, 1996. **46**(3): p. 965-972.

2. Bourbigot, S., et al., *Characterization of the morphology of iPP/sPP blends with various compositions.* eXPRESS Polymer Letters, 2013. **7**(3).

3. Romão, W., et al., *Distinguishing between virgin and post-consumption bottle-grade poly (ethylene terephthalate) using thermal properties.* Polymer Testing, 2010. **29**(7): p. 879-885.

4. Spinacé, M.A.S. and M.A. De Paoli, *Characterization of poly(ethylene terephtalate) after multiple processing cycles.* Journal of Applied Polymer Science, 2001. **80**(1): p. 20-25.

5. Michaeli, W. and T. Schmitz, *Pet Film Extrusion with Degassing.* Journal of Polymer Engineering, 2006. **26**(2-4): p. 147-160.

6. Fávaro, S.L., et al., *Surface modification of HDPE, PP, and PET films with KMnO4/HCl solutions.* Polymer Degradation and Stability, 2007. **92**(7): p. 1219-1226.

7. Li, Y., et al., *Contact Angle of Water on Polystyrene Thin Films: Effects of CO2 Environment and Film Thickness.* Langmuir, 2007. **23**(19): p. 9785-9793.

8. Socrates, G., *Infrared and Raman characteristic group frequencies: tables and charts*. 2004: John Wiley & Sons.

9. Kovacevic, A., et al., *Polyhydroxy surfactants for the formulation of lipid nanoparticles (SLN and NLC): Effects on size, physical stability and particle matrix structure.* International Journal of Pharmaceutics, 2011. **406**(1): p. 163-172.

10. Balog, S., et al., *Characterizing nanoparticles in complex biological media and physiological fluids with depolarized dynamic light scattering.* Nanoscale, 2015. **7**(14): p. 5991-5997.

11. Rifaie-Graham, O., et al., *The Kinetics of β-Hematin Crystallization Measured by Depolarized Light Scattering.* Small, 2018. **14**(46): p. 1802295.

12. Bossert, D., et al., *Hypothesis test of the photon count distribution for dust discrimination in dynamic light scattering.* Analytical chemistry, 2018. **90**(6): p. 3656-3660.

13. Bossert, D., et al., *Speckle-visibility spectroscopy of depolarized dynamic light scattering.* The Journal of Physical Chemistry B, 2017. **121**(33): p. 7999-8007.

14. Geers, C., et al., *A new angle on dynamic depolarized light scattering: number-averaged size distribution of nanoparticles in focus.* Nanoscale, 2016. **8**(34): p. 15813-15821.

15. Mohr, K., et al., *Evaluation of multifunctional liposomes in human blood serum by light scattering.* Langmuir, 2014. **30**(49): p. 14954-14962.

16. Moore, T.L., et al., *Nanoparticle colloidal stability in cell culture media and impact on cellular interactions.* Chemical Society Reviews, 2015. **44**(17): p. 6287-6305.

17. Rausch, K., et al., *Evaluation of nanoparticle aggregation in human blood serum.* Biomacromolecules, 2010. **11**(11): p. 2836-2839.

18. Reipa, V., G. Purdum, and J. Choi, *Measurement of nanoparticle concentration using quartz crystal microgravimetry.* The Journal of Physical Chemistry B, 2010. **114**(49): p. 16112-16117.